ELSEVIER

Journal of Structural Geology 27 (2005) 433–445

JOURNAL OF STRUCTURAL GEOLOGY

www.elsevier.com/locate/jsg

Sandbox experiments on basin inversion: testing the influence of basin orientation and basin fill

Marion Panien*, Guido Schreurs, Adrian Pfiffner

Institute of Geological Sciences, University of Bern, Baltzerstrasse 1-3, CH-3012 Bern, Switzerland

Received 11 March 2004; received in revised form 12 October 2004; accepted 5 November 2004

Abstract

Analogue modelling experiments using brittle materials are performed to study the inversion of extensional structures. Asymmetric grabens of two different orientations are first created during a phase of extension and progressively filled. They are subsequently shortened in the same direction. The aim of our experiments is to determine factors affecting the style of deformation during inversion. We specifically investigate variations in thickness and distribution of strong and weak layers constituting the graben fill and in initial basin orientation. The main advantage of our experimental set-up is that we have a complete control on graben location, width, infill and orientation before inversion. The experiments show that shortening results only in limited reactivation of pre-existing normal faults. In general, forward thrusts and backthrusts cut across normal faults into the footwall of the graben. The forward thrusts either propagate parallel to the enveloping surface of faulted blocks or they cut across basin-limiting normal faults at various angles. The graben fill is mechanically extruded by displacement along forward thrusts that accommodate most of the shortening. Both pre-existing faults and weak graben fill act as zones of weakness during inversion and determine the orientation and location of both backthrusts and forward thrusts. The results of our experiments conform well to natural examples of inverted graben structures.

Keywords: Basin inversion; Asymmetric graben; Basin orientation; Basin fill

1. Introduction

Analogue modelling has been used since the nineteenth century to simulate natural geological structures with the aim of understanding the mechanisms controlling their geometry and kinematics. In this study, we focus on analogue models of basin inversion. Many previous analogue experiments on basin inversion have investigated hanging wall deformation using rigid footwalls. The footwall blocks usually represent a structural basement with faults of varied geometries, e.g. listric, planar or ramp/flat listric. The deformable hanging-wall made of sand, clay, or sand and clay mixtures is first extended and then contracted (McClay, 1989, 1995; Buchanan and McClay, 1991; McClay and Buchanan, 1992; Keller and McClay, 1995; Yamada and McClay, 2003). In these experiments, inversion results in both the reactivation of the main detachment and the initiation of new thrust faults. Inversion has also been achieved by uplift and rotation of a single rigid 'basement' block (Koopman et al., 1987) or by a series of rigid metal plates simulating rigid domino fault blocks (Buchanan and McClay, 1992; McClay and Buchanan, 1992; Mitra, 1993; Vially et al., 1994; Roure and Colletta, 1996). Reactivation of the normal faults is in this case again strongly influenced by the movement of the rigid blocks. A disadvantage of these models is the formation of rigid footwalls, basement blocks and metal plates that are unable to deform.

Other analogue experiments have allowed both footwall and hanging wall to deform freely. A graben-bounding master fault is initiated by a velocity discontinuity localised at the base of the model. This velocity discontinuity is created by the displacement of two overlapping basal plates. One of the basal plates is fixed to the mobile wall whereas

* Corresponding author. Tel.: +41-31-631-48-32; fax: +41-31-631-48-43

E-mail address: panien@geo.unibe.ch (M. Panien).

0191-8141/$ - see front matter © 2005 Elsevier Ltd. All rights reserved.
doi:10.1016/j.jsg.2004.11.001

the other is attached to the stationary wall. This particular set-up was used to study the geometry and kinematic evolution of structures in both extension and inversion models. In the experiments of Cloos (1968) and McClay and Ellis (1987) extension resulted in the formation of an asymmetric graben. In the inversion experiments of Eisenstadt and Withjack (1995) using wet clay, early shortening was accommodated by reverse displacement along the main normal faults. During further shortening, these reactivated normal faults are cut by low-angle thrust faults. No reactivation was observed in the clay models of Mitra and Islam (1994). Instead, initial shortening resulted in the uplift of the graben boundaries and in footwall deformation. Using the same experimental set-up, but with brittle and viscous analogue materials, Brun and Nalpas (1996) assessed the effects of obliquity between the direction of shortening and the graben axis. They showed that this obliquity had to be less than 45° to allow graben inversion and fault reactivation.

Our study is based on basin inversion experiments in which both the footwall and hanging wall are free to deform. These experiments use only granular materials as analogues for upper crustal rocks. Using a velocity discontinuity at the base, models are first extended and then shortened in the same direction. The extensional phase leads to the formation of an asymmetric graben that is progressively filled using materials of different strengths. Based on the fact that sedimentary deposits in basins are generally less competent than adjacent basement rocks, part of the graben fill consists of granular materials that are weaker than the surrounding material.

The aim of our experiments is to identify factors affecting the style of deformation and contributing to reactivation of the graben-bounding normal faults during inversion. We investigate the thickness and distribution of strong and weak layers constituting the graben fill and the pre-inversion basin orientation. In our experimental set-up we have complete control of graben location, width, infill and orientation before inversion. The experimental results are compared with other model studies and with natural examples.

2. Scaling and modelling materials

Deformation structures in analogue models generally are smaller, develop in a much shorter time, and require less force than structures in nature. Analogue models, therefore, must be scaled in such a way that similarity between the model and a natural example is as close as possible. The theory of mechanical scale models was applied to geological structures by Hubbert (1937, 1951) and Ramberg (1981), who derived a set of scale ratios between the mechanical properties of the model and the corresponding properties of the natural object. Dynamic similarity of the surface forces must be maintained for proper scaling and requires that both analogue material and natural (rock) material must have similar mechanical properties (cf. Weijermars and Schmeling, 1986). In general, upper crustal rocks are assumed to deform according to the Coulomb failure criterion, which implies a time-independent rheological behaviour and can be described by:

$$\tau = C_0 + \sigma\mu \quad \text{where} \quad \mu = \tan\phi$$

where C_0 = cohesion, σ = normal stress, τ = shear stress, μ = coefficient of internal friction, and ϕ = angle of internal friction.

As ratios of length and time are independent ratios, we can then choose ratios suitable for our experiment.

In our experiments, quartz sand, corundum sand and microbeads are used as analogue materials. The size of the grains varies between 80 and 200 μm for quartz sand, between 88 and 125 μm for corundum sand and between 70 and 110 μm for microbeads. We determined the mechanical properties of each of these granular materials using a ring shear tester (Schulze, 1994). Several authors have shown that the standard assumption that granular materials are ideal cohesionless Coulomb-materials with constant frictional properties is inadequate (Lohrmann et al., 2003; Panien 2004). In our ring-shear tests, friction was determined for three different states: at the onset of failure (first peak strength), at the moment of fault reactivation (second peak strength) and once a fault is formed or reactivated (dynamic-stable strength) (Table 1 and Fig. 1). The cohesion values are difficult to estimate for the low normal stresses found in our models. Repeated ring-shear tests on the same analogue material revealed widely varying cohesion values. According to shear tests made by Schellart (2000), granular materials have negligible cohesion at very low normal stresses (<400 Pa).

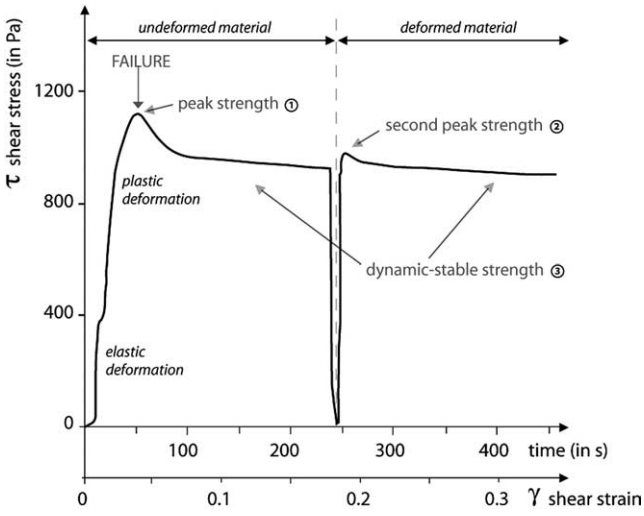

Fig. 1. Shear stresses (τ) variations plotted as a function of shear strain (γ) and time obtained with a ring-shear tester for corundum sand using a normal load of 3 kg. The numbers (1, 2 and 3) correspond to the numbers of Table 1.

Table 1
Angle and coefficient of friction and strain-softening values of quartz sand, corundum sand and microbeads. The strain softening is the difference between the coefficients of first peak strength and dynamic-stable strength divided by first peak strength. The values of coefficient and angle of friction have been rounded off

	Quartz sand		Corundum sand		Microbeads	
Angle ϕ and coefficient of friction μ at:	ϕ	μ	ϕ	μ	ϕ	μ
1. First peak strength	35.5	*0.71*	37.0	*0.75*	22.3	*0.41*
2. Second peak strength	33.3	*0.66*	33.8	*0.67*	21.9	*0.40*
3. Dynamic-stable strength	31.2	*0.61*	32.2	*0.63*	20.6	*0.37*
Strain softening (%)	14		16		9.7	

Our ring-shear test results indicate that quartz and corundum sand have peak friction angles of 35.5 and 37°, respectively, similar to those determined experimentally for competent upper crustal rocks (e.g. Byerlee, 1978). Microbeads with a peak friction angle of 22° are much weaker and are used to simulate weak rocks like (over-pressured) shales. Experimentally derived stress–strain curves for natural rocks occurring in the upper brittle crust (Barnhoorn et al., 2004), although more diverse, are very similar to the stress–strain curves for our analogue materials. Both brittle crust and analogue materials are characterised by an elastic frictional–plastic material behaviour with an initial strain-hardening phase preceding failure that is followed by a transitional phase of strain-softening until stable sliding (Lohrmann et al., 2003).

Modelling generally involves simplifications and assumptions about the mechanisms of rock deformation in nature. Limitations of our basin inversion experiments include the neglect of pore fluid pressures and the absence of thermal gradients with depth. Pore fluid pressure in particular may exert an important control on brittle fault reactivation (Sibson, 1985; Etheridge, 1986). What is important, however, is that the ring shear tests show that there is a strength contrast between the faults and the surrounding unfaulted material. Strain softening (i.e. the difference between the coefficients of first peak strength and dynamic-stable strength divided by first peak strength) of about 15% occurs along faults that remain active (Fig. 1). It is clear that, in the presence of high pore fluid pressure, the contrast in strength between faulted and unfaulted material could be significantly higher.

3. Model set-up and experimental procedure

The models are built in a wooden sandbox and deformed by moving one of the vertical walls of the sandbox at a constant velocity of 2.4 cm/h for both extension and shortening. Application of the non-destructive X-ray computed tomography (CT) technique makes it possible to visualise the interior of our analogue models without destroying them. The CT scanner measures the attenuation of X-rays that go through the model. Attenuation values given in Hounsfield units depend on mineralogical composition, grain size and material compaction. In order to visualise layering within a model, quartz and corundum sand are used. These materials have similar mechanical properties but different attenuation values. Iodine powder with a high X-ray attenuation was sprinkled on top of each layer. The tiny marker particles do not have any influence on the properties of the surrounding granular material. They appear as bright dots on X-ray images and allow us to construct displacement paths. The 3D volume raw data acquired by X-ray CT is post-processed using software with which computer animations of the spatial and temporal evolution of the models can be created. This permits a detailed analysis of the internal 3D geometry and kinematics of analogue models (e.g. Mandl, 1988; Colletta et al., 1991; Schreurs et al., 2003).

Models consist of alternating layers of quartz and corundum sand that are sieved from a height of 20 cm into the sandbox to obtain three horizontal layers, each 1 cm thick. Before extension, the model is 30 cm long, 25 cm wide and 3 cm thick (Fig. 2a). As the failure properties of the materials vary significantly depending on the handling technique employed (Krantz, 1991; Lohrmann et al., 2003), layers are sieved at a constant filling rate. A basal décollement consisting of a 0.5-mm-thin layer of microbeads is included at the base of the model. It reduces the basal friction from initially 20.5 to 12.5° and thus ensures stress transmission during shortening. A velocity discontinuity is created at the base of the model by using a plastic sheet that underlies part of the model and is fixed to the mobile wall (Fig. 2a).

During extension, the part of the model covering the plastic sheet is carried away whereas the other part of the model does not move. Between these two parts, conjugate faults dipping at 60° are initiated at the edge of the plastic sheet. By changing the shape of the plastic sheet, the initial graben orientation can be varied. The right-hand master fault is passively transported by the plastic sheet, whereas the other fault is tilted by a few degrees and then becomes inactive. New antithetic faults are then progressively formed in the hanging wall of the master fault to accommodate further extension. This results in the formation of a fault array, delimiting several fault blocks. At the end of extension the two sides of the graben are different. The layers situated in the subsiding graben slid down the master fault plane onto the base of the model. After each centimetre of extension, granular materials are sieved into the graben to

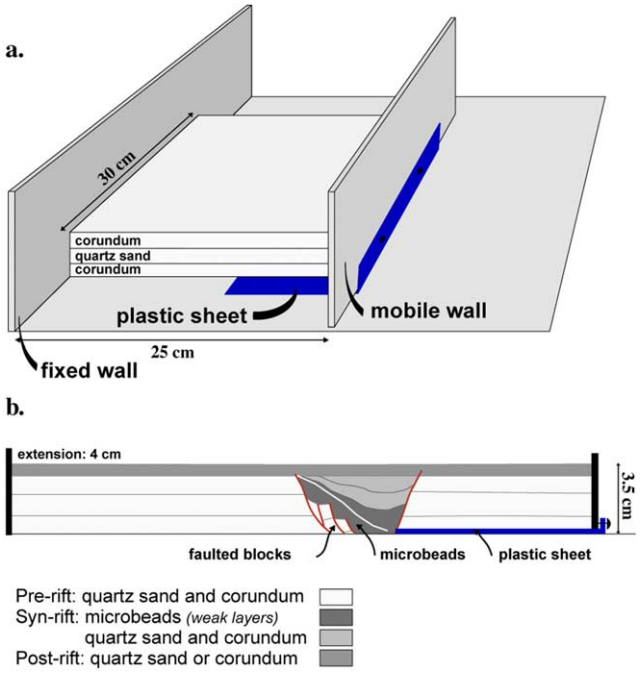

Fig. 2. Experimental set-up. (a) Drawing of experimental apparatus, showing a cross-section view of the undeformed three-layer model above the plastic sheet fixed to the mobile wall. (b) Schematic representation of model after 4 cm of extension. Sprinkled iodine powder (white line) is situated in between the two layers of microbeads. The plastic sheet was detached from the mobile wall before shortening.

simulate syn-extensional sedimentation. Brittle materials of alternating strength (Table 1) are used to progressively fill the graben. Because of the collapse of the layers during extension, the graben fill has a synclinal shape and thins towards the graben shoulders. After 4 cm of extension, the experiment is halted and an additional 0.5-cm-thick layer of sand is sieved on top to simulate a post-rift sequence (Fig. 2b). The plastic sheet is detached from the mobile wall before the onset of shortening. The same experiment was run at least twice to ensure reproducibility.

4. Modelling results

4.1. Normal graben versus oblique graben

Two experiments were performed to test the influence of the orientation of the graben with respect to the direction of extension/shortening on the resulting structures In the first experiment, the edge of the plastic sheet (and thus the basal velocity discontinuity) is parallel to the mobile wall whereas in the second experiment, the edge of the plastic sheet makes an angle of 30° with the mobile wall (Fig. 3). In both experiments, the graben-fill consists of two layers of microbeads overlain by one layer of corundum sand and another one of quartz sand. The microbead layers are separated from one another by sprinkled iodine particles that act as passive markers. At the end of extension the graben geometry as seen in vertical sections is similar in the two experiments (Fig. 3c); however, the orientation of the grabens is different: parallel to the mobile wall in the first experiment (referred to as normal graben, NG, experiment) and at an angle of 30° in the second experiment (referred to as oblique graben, OG, experiment).

4.1.1. Shortening of normal graben (NG)

During shortening of the NG model, deformation is mostly accommodated by folding, faulting and uplift of the graben fill Vertical cross-sections of the model obtained by X-ray CT are shown in Fig. 4. The normal fault closest to the mobile wall is partly reactivated. It propagates upwards to the surface through the post-rift sequence at a shallower angle and a new fault branches off this reactivated fault (short-cut fault). The extensional fault on the opposite side of the graben is not reactivated. Instead a forward thrust (dipping towards the mobile wall) initiates in the weak

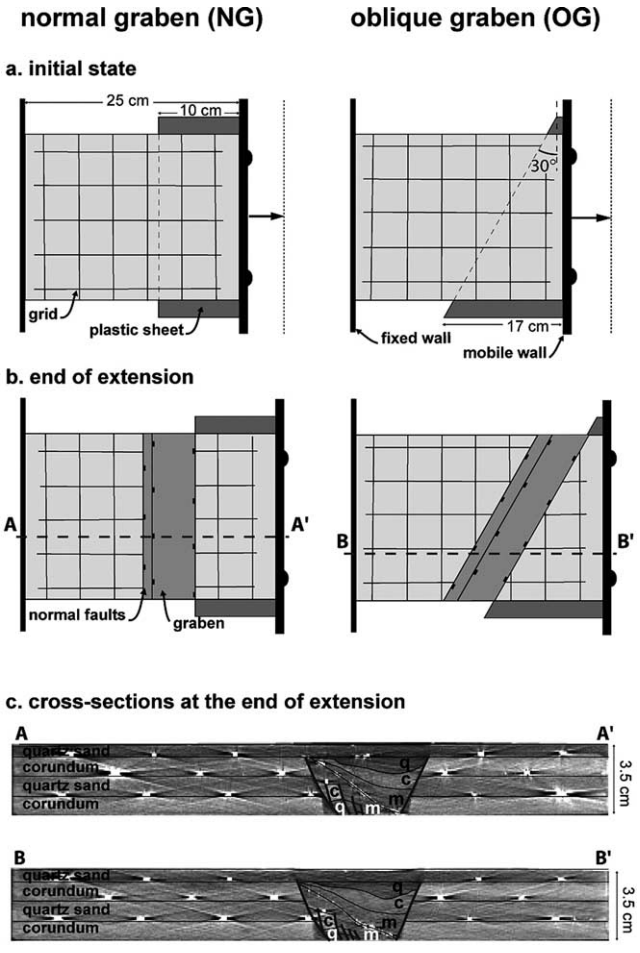

Fig. 3. Normal graben (NG) and oblique graben (OG) experiments. Map view of the NG and OG experiments at the initial undeformed state (a) and after 4 cm of extension (b). (c) X-ray CT images of cross-sections after 4 cm of extension. Iodine markers appear as bright spots. The crosses around these spots are artefacts due to the strong X-ray absorption of iodine. Layering is shown as thin lines, faults as thick lines. Location of cross-sections is given in (b). q = quartz sand, c = corundum and m = microbeads.

microbeads filling the graben, following the enveloping surface of the faulted blocks (Fig. 4b) and propagating across the post-rift sequence to the surface. This results in the formation of a fold with an inverted limb in the weak graben fill, which will be discussed in more detail later. In parts of the model, one corner of the faulted blocks is cut and carried away by the forward thrust. The graben fill is progressively uplifted reaching a stable surface slope of 35° above the tip of the thrust. This slope angle corresponds to the angle of repose of sand. Once this maximum angle is reached, granular material slides down resembling slope-dependent erosion. With increasing deformation the graben-bounding block closest to the mobile wall starts to deform by a series of in-sequence backthrusts. The graben-bounding block (on the right) is passively transported by the forward thrust and is rotated. Backthrusts are formed successively in this block in response to the change in orientation from lower flat to ramp. The backthrusts cease their activity one after the other as their dips decrease during transportation along the forward thrust (Fig. 4c–e).

For the calculation of the displacement paths of several marker particles during shortening, the fixed wall of the sandbox (on the left-hand side) is taken as a reference (Fig. 5). Three spatially separated patterns of deformation can be defined (Fig. 5a). (1) Markers situated in the left-hand side of the model show only a small amount of displacement. It increases during the last stages of shortening as the graben fill is mechanically extruded and deformation propagates toward the left-hand side of the model. Displacement magnitudes decrease from the border fault of the graben toward the fixed wall and underline the lateral gradient in

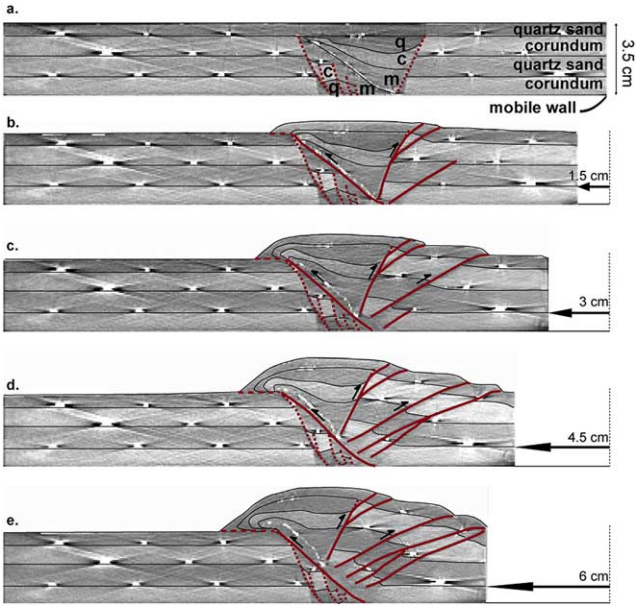

Fig. 4. X-ray CT images of NG model: (a) before shortening, (b) after 1.5 cm, (c) 3 cm, (d) 4.5 cm, and (e) 6 cm shortening. Layering is shown as thin lines, faults as thick lines; dashed lines for normal faults, continuous lines for reverse faults. Half-arrows indicate relative displacement along faults. q = quartz sand, c = corundum sand and m = microbeads.

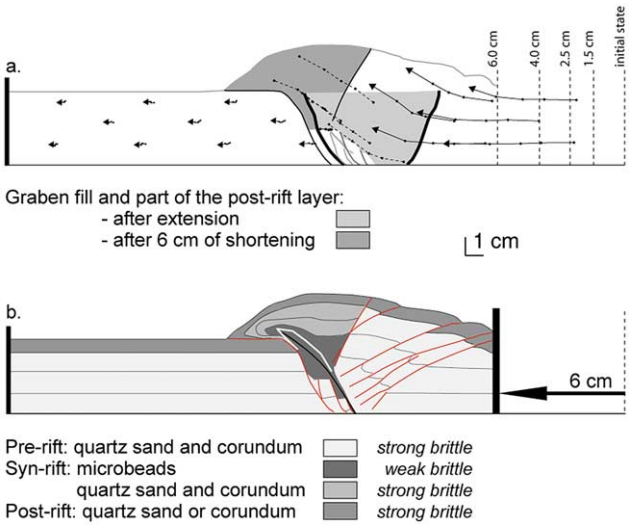

Fig. 5. Evolution of the NG experiment. (a) Particle paths of iodine markers during shortening of NG model constructed with reference to the fixed wall (left-hand side). Particle paths located inside the graben are shown as dashed lines, those outside the graben as continuous arrows. Vertical dotted lines represent the successive location of the mobile wall during progressive shortening. The thick and thin solid lines refer to the graben-bounding fault at the initial stage and after 6 cm of shortening, respectively. (b) Cross-section of the NG experiment after 6 cm of shortening. The grey lines represent reverse faults and previous normal faults. The forward thrust is shown as a black line and the iodine markers as a white line.

compaction. (2) Markers initially near the right-hand side of the model move predominantly horizontally with no or a very small component of upward translation at the end of deformation, due to the formation of backthrusts. (3) Markers situated close to the right-hand graben-bounding fault and inside the graben fill show arcuate displacement paths. They move sub-parallel to the enveloping surface of the faulted blocks, and thus parallel to the forward directed thrust surface.

4.1.2. Shortening of oblique graben (OG)

During the early stages of shortening of the OG model, the footwall of the graben closest to the mobile wall acts as a rigid block after initial compaction It transmits the horizontal displacement produced by the mobile wall to the graben and the graben fill begins to bulge upwards (Fig. 6). Further shortening results in partial reactivation of the normal fault closest to the mobile wall with the development of a footwall shortcut that continues as a backthrust in the previously undeformed post-rift quartz sand layer. On the other side of the graben, a forward thrust uses the enveloping surface of the faulted blocks and cuts through the post-rift layer. The emerging forward- and backthrusts are oblique to the mobile wall, but parallel to the oblique graben-bounding faults. As the inverted graben is mechanically extruded, the footwalls on either side start to deform. A backthrust forms in the footwall near the mobile wall. It roots at the base of the model where there is a change from strong to weak brittle materials and reaches the surface next

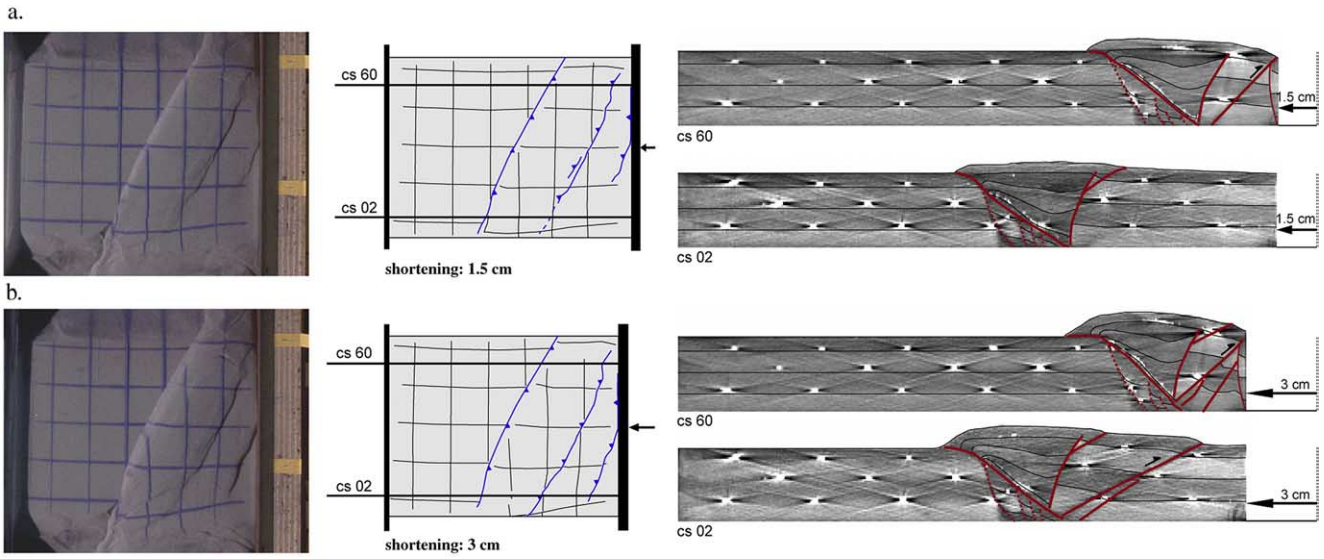

Fig. 6. Map views of progressive deformation and vertical sections of the oblique graben (OG) experiment. (a) After 1.5 cm of shortening. Uplift develops between the two oblique graben-bounding faults that are partially reactivated. A backthrust appears near the mobile wall and propagates laterally. (b) After 3 cm of shortening. Backthrust near mobile wall extends along the entire model.

to the mobile wall. This backthrust does not form simultaneously in the whole model, but first initiates in the region where the graben is closest to the mobile wall. It propagates laterally during further shortening and is oblique to the mobile wall. At the end of the experiment, the amount of displacement and uplift of the graben and its bounding-faults varies as a function of its lateral position in the model.

Particle displacement paths in vertical sections (Fig. 7a) illustrate that the translation of the graben decreases with its distance from the mobile wall. In cross-sections 60 and 40 (cs 60, cs 40; Fig. 7a), the initial oblique graben was close to the mobile wall. Here, shortening is immediately localised in the graben, extruding the basal weak graben-fill and overlying stronger material upward along forward- and backthrusts. When most of the weak basin fill has been extruded to higher levels, mainly by displacement along the forward thrust, the stronger material of both footwalls comes into close proximity in the lower part of the model. It is inferred that stresses are now more easily transmitted across the model, resulting in a substantial translation of the left-hand major graben-bounding fault and the material in its footwall by diffuse deformation. This deformation propagates towards the front of the model. Note also the slight upward component in the displacement paths during the last stages of shortening, suggesting that the development of a second in-sequence forward thrust was imminent. In contrast, in sections cs 20 and cs 02 of Fig. 7 the initial oblique graben was further away from the mobile wall and backthrusts reach the surface. Therefore, at identical stages of shortening, less graben fill was extruded suggesting that stresses were less easily transmitted through the model. The left-hand graben-bounding fault and its footwall, therefore, experienced less deformation.

The final geometry of the structures also reflects the initial position of the graben with respect to the mobile wall. In sections cs 60 and cs 40 the deformation occurs over a narrower zone, whereas in cs 20 and cs 02 the zone of deformation is broader due to the activity along backthrusts (Fig. 7a and b).

4.1.3. Comparison between normal graben (NG) and oblique graben (OG) experiments

The orientation of the graben and the strength of its fill have an important influence on the resulting structural style during shortening The weak basin fill at the base of the graben localises the position of the forward thrust, the partial reactivation of the right-hand graben-bounding normal fault and its upward propagation as backthrust in the post-rift layer. Contractional faults nucleate at the basal transition from weak to strong brittle layers. In the oblique graben experiment, this transition strikes at 30° to the mobile wall. Graben fill extrusion and backthrusts consequently also develop oblique to the shortening direction in contrast to shortening of the normal graben. Moreover the obliquity of the initial graben causes lateral changes along strike in the overall cross-sectional geometry: from relatively narrow uplifted domains bounded by contractional faults to broader uplifted domains.

A comparison between NG and OG experiments reveals that the evolution of structures in cross-sections is similar when the initial distance between the graben and mobile wall is the same. This similarity is expressed by the nearly identical particle displacement paths shown in Figs. 5 and 7 (cs 02) and by similar fault architectures at the end of shortening.

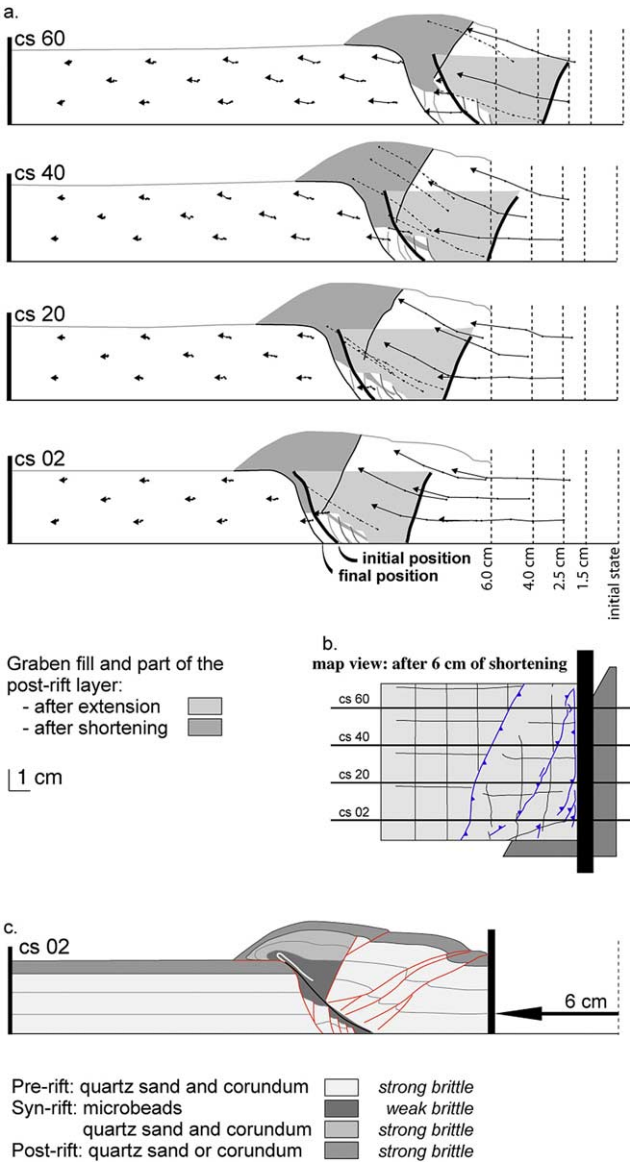

Fig. 7. Oblique graben (OG) experiment in sections and in map view. (a) Particle displacement paths are constructed with reference to the fixed left-hand wall. The vertical dashed lines represent the successive location of the mobile wall during shortening. The continuous arrows and dashed lines illustrate displacement paths of markers situated in the graben-bounding blocks and in graben fill, respectively. Solid lines mark the initial position of the graben-bounding faults, thin lines their position at the end of the experiment. (b) Position of the four vertical sections shown in (a). (c) Cross-section (cs 02) after 6 cm of shortening.

4.2. Variable graben fill

Based on the normal graben (NG) set-up, additional experiments were conducted to test the effect of various graben fills on the structures resulting from shortening. In three different experiments, the position of a weak layer of microbeads in the graben was either at the base (NGwb = NG, weak base), in the middle (NGwm = NG, weak middle) or at the top (NGwt = NG, weak top). In a fourth experiment (NGab = NG, all brittle), the graben was only filled with strong brittle layers. The overall geometry of the pre-shortening model was similar for all the experiments.

The deformation style during shortening is quite similar for all models (Fig. 8). However, the dip and the location of the thrusts vary between the different models. During the first stages of shortening, the normal fault closest to the mobile wall is partly reactivated and propagates upwards to the surface through the post-rift sequence. A thrust fault, first initiated in the graben at the base of the weak layer, propagates upward and downwards through the model, cutting into the footwall (Fig. 8). A conjugate backthrust is produced at almost the same time. The location of the forward thrust strongly depends on the position of the weak layer inside the graben. In experiments NGwb, NGwm, and NGwt, the forward thrust was localised in the lower part of the weak layer, whereas in experiment NGab, the thrusts were localised at the base of the first and the third layers constituting the graben fill. The dip of forward- and backthrusts is not the same for all experiments but depends on the mechanical stratigraphy of the graben fill. The forward thrusts dip between 23.5 and 38.6°, whereas backthrusts dip between 30 and 39.7°. The higher the relative position of the weak syn-rift graben fill, the lower the initial dip of the forward thrust. The angle between the conjugate faults in the four experiments, however, remains almost equal, between 110 and 119°.

Further shortening leads to the formation of an in-sequence forward thrust that cuts the left graben-bounding fault of experiments NGwm, NGwt and NGab. It also results in the formation of a fold with an inverted limb in the weak graben fill of experiments NGwb, NGwm and NGwt (Fig. 8a–c). The shape of the inverted grabens is asymmetric with a forward vergence in these experiments, whereas in experiment NGab, the shape is more symmetrical. With increasing shortening, several backthrusts appear in all experiments. These faults cease their activity one after the other as they are passively carried by the forward thrust faults.

The displacement paths of several marker particles are plotted in Fig. 9 using the technique previously described. They allow the identification of three spatially separated patterns of deformation in all four experiments, similar to those described for the shortening of the NG model (Section 4.1.1). In addition, a fourth pattern can be observed in experiments NGwm and NGab. Outside the graben, markers next to the left graben-bounding fault have an upward component at the end of the deformation. This is due to the formation of a second in-sequence forward thrust, which cuts through the graben-bounding fault. This pattern would also have been observed in experiment NGwt if more markers had been dispersed in the proximity of the left graben-bounding fault.

4.3. Kinematics of graben-fill extrusion

As previously mentioned, the propagation of the forward

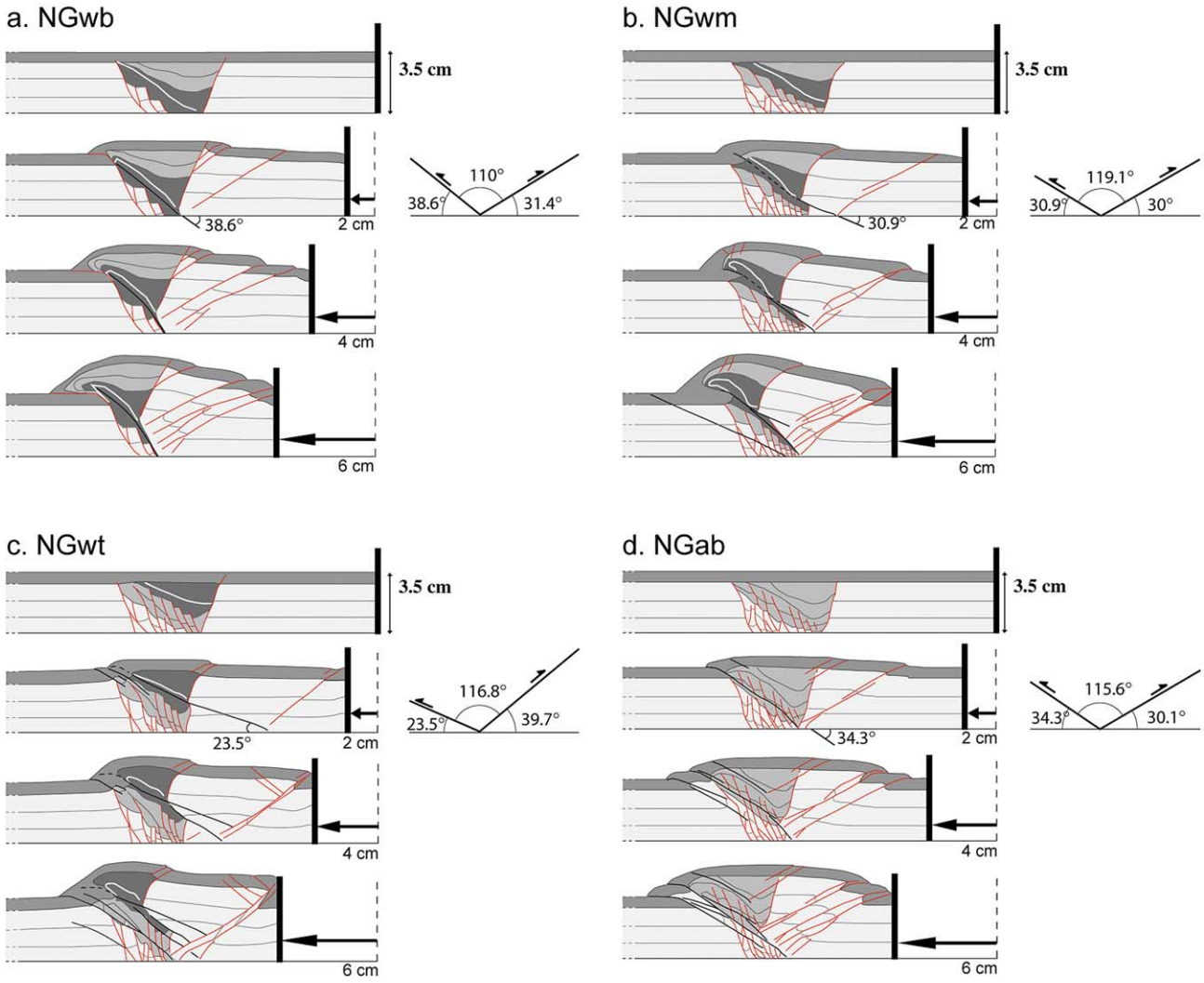

Fig. 8. Cross-sections of four NG experiments showing the evolution in four steps from the initial state (i.e. after extension) until 6 cm of shortening. Line-drawing after CT images. Only central parts of the models are shown. The graben was filled with a weak brittle layer at the base (NGwb) (a), in the middle (NGwm) (b) and at the top (NGwt) of the graben (c). A fourth was only filled with strong brittle materials (NGab) (d). White line in weak graben fill represents iodine powder trace, the black lines are the forward thrusts and the grey lines the backthrusts. For each experiment, conjugate thrusts formed at nearly identical stages of shortening. The location and dip of these thrusts depends on the graben fill.

thrust along the enveloping surface of the faulted blocks in the graben results in the formation of a fold with an inverted limb in the weak graben fill (Fig. 10). Markers within the graben follow arcuate displacement paths as they are transported by the forward thrust. Iodine markers placed in between the two syn-rift microbeads layers show the internal deformation of the weak layer for four successive stages of shortening (Fig. 10c). The distance between adjacent marker particles (segments **ab**, **bc**, **cd**, **de**, **ef** and **fg**) has been measured for different stages of shortening in the NGwb experiment and is plotted in Fig. 10b. The initially highest marker (**a** in Fig. 10c, initial stage) is taken as a 'fixed point'. Other marker particles gradually roll past this 'fixed point' and form a fold. Line segments **ab** and **bc** experience first a reduction in length of more than 60% (Fig. 10b). As marker particles **b** and **c** overtake marker particle **a**, segments **ab** and **bc** are successively stretched and at the end of the experiment, segment **ab** has regained its initial length. This evolution suggests that the fold evolved by hinge roll and that the inverted limb of the fold was stretched during progressive shortening.

The formation of the fold in the weak microbeads is directly linked to the progressive evolution of a relatively broad shear zone (forward-directed thrust) that is oblique to the iodine layer and follows the enveloping surface of the faulted blocks in the course of its upward propagation. From a close observation of the relative displacements of the iodine markers, one can deduce that the shear zone is composed of at least three parallel forward thrusts, which develop progressively into the hanging-wall. The first thrust is localised between particles **a** and **b**, the second between **b** and **c** and the third between **c** and **d** (Fig. 10c). Line segments **de** and **ef** do not show large fluctuations in length during inversion indicating that they remained outside of the main forward shear zone. They were passively transported in the

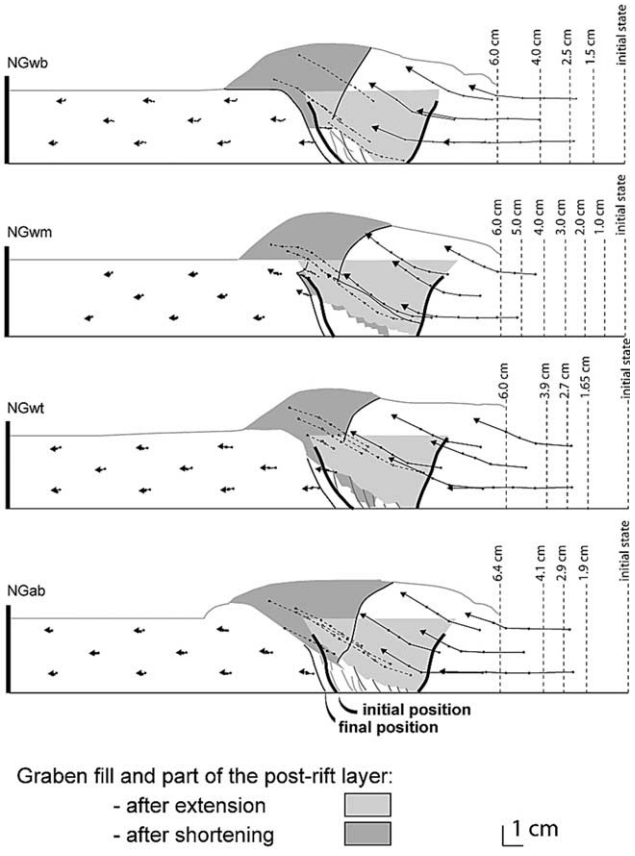

Fig. 9. Particle displacement paths in NGwb, NGwm, NGwt and NGab experiments during shortening. Particle paths are constructed with reference to the fixed left-hand wall. Vertical dashed lines represent the successive location of the mobile wall. Continuous arrows and dashed lines are for markers situated in the graben-bounding blocks and in graben fill, respectively. Solid lines mark the initial position of the graben-bounding faults, thin lines their position at the end of the experiment.

hanging-wall of the forward thrusts. The displacement of marker **g** is different from the other particles in that it first experiences a horizontal displacement path that then points upward (Fig. 5). Marker **g** was pushed by the right graben-bounding fault because of the shortening of the model. The horizontal shortening also leads to the progressive bending of the shear zone. Between 2 and 4 cm of shortening, marker **g** is displaced into the shear zone, between thrusts 2 and 3. The contemporaneous activity of thrusting and folding with development of an inverted limb is reminiscent of a fault propagation fold.

5. Discussion

The results of our experiments and their comparison to natural examples at different scales can help to improve our understanding of inversion related structures that form during progressive shortening of a previous extensional basin.

5.1. Upward bulging

Shortening of the extensional graben in the models is first accommodated by the upward bulging of its fill and cover regardless of the composition of the fill or the graben orientation Chadwick (1993) shows that inversion in the Wessex Basin (southern England) also occurs by bulk shortening of the graben-fill to produce a regional upwarp (Fig. 11). He suggests that this takes place by a combination of pure-shear shortening and localised minor reverse faulting in the young, poorly lithified and therefore relatively weak graben-fill sediments. Chadwick (1993) considers that horizontal shortening at depth is progressively transformed into predominantly vertical motion in the shallower parts of the basin.

5.2. Fault reactivation

Reactivation of normal faults during shortening in our experiments is limited and occurs—if at all—along the main normal fault closest to the mobile wall Brun and Nalpas (1996) demonstrate that in orthogonal shortening reactivation of normal faults dipping at 60° is not possible in purely brittle systems. Instead, their experiments show that new reverse faults develop outside the graben dipping between 30 and 40°. Normal faults are only reactivated as oblique-slip faults if the angle between the compression and the graben trend is smaller than 45° (Brun and Nalpas, 1996). During shortening of our oblique graben experiment, there is no strike-slip movement between the graben structure and the rest of the model although the graben made an angle of only 30° with the mobile wall. In the models of Brun and Nalpas (1996), shortening is applied by the displacement of a basal plate that ends directly beneath the graben. This strongly localises the deformation inside the graben. Using this set-up, it is thus possible to obtain transpression inducing graben reactivation. Our experiments are less constrained as shortening is applied by displacement of the mobile wall. This leads to the progressive compaction of the right-hand part of the model before deformation of the graben. In both our NG and OG experiments, extension and subsequent shortening share the same direction. The major difference with previously published experiments consists of the use of materials with varying mechanical strength: grabens are partly filled with less competent materials than those delimiting the graben.

Sibson (1985) suggests that the reactivation of normal faults (dipping at 60°) as high-angle reverse faults in nature is possible under certain specific conditions, e.g. when the friction value for fault reactivation is less than 0.55. The friction values of quartz sand and corundum sand for fault reactivation (second peak strength) are lower than friction values for fault initiation but still greater than the threshold value ($\mu = 0.55$) calculated by Sibson (1985). This could explain why there is no reactivation of the normal fault closest to the mobile wall when the graben is only filled with

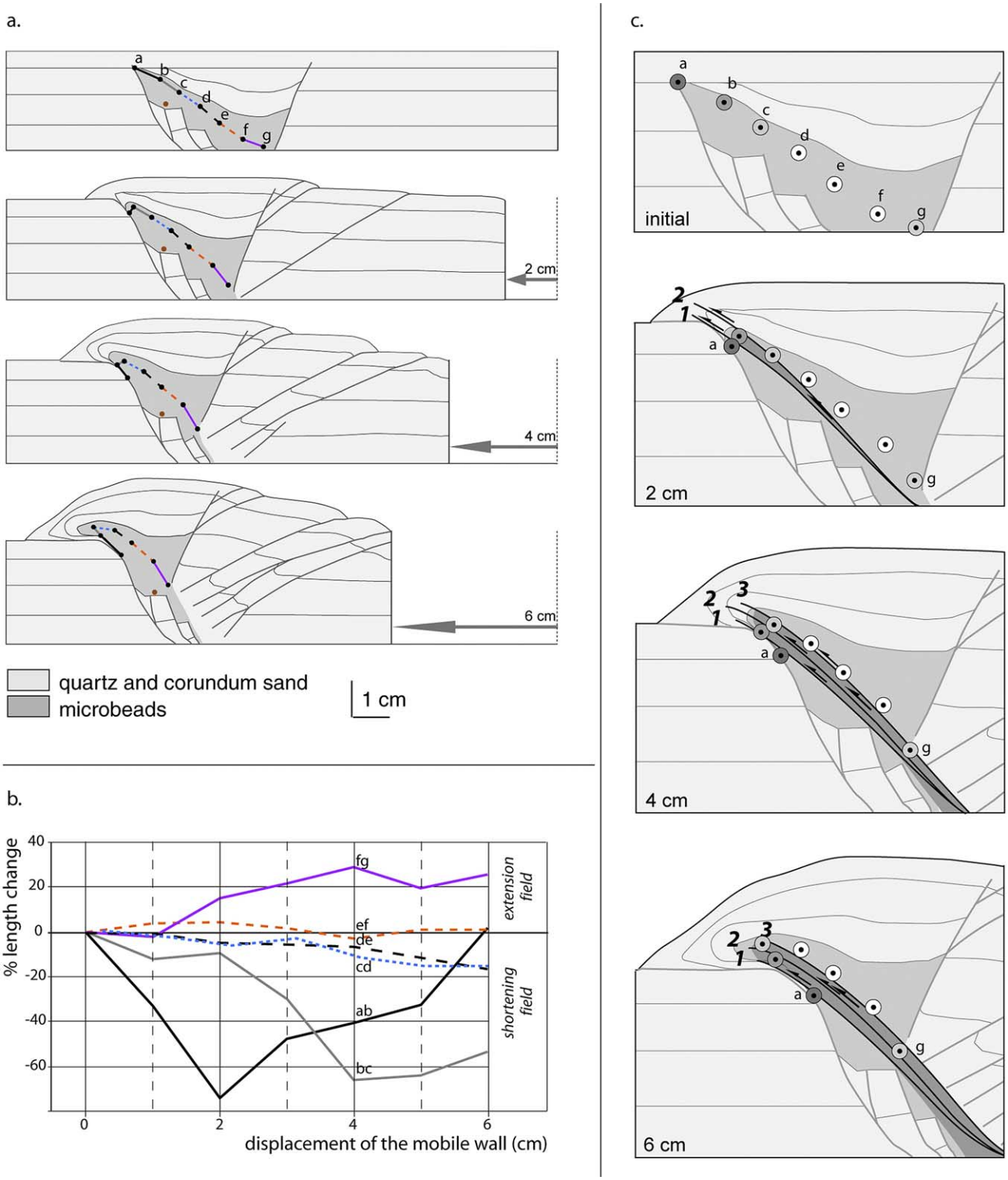

Fig. 10. Kinematic interpretation of inversion in NG experiment. (a) Displacement of iodine markers during progressive shortening. The granular iodine markers were sprinkled in between two syn-rift microbeads layers. (b) Length changes between two neighbouring marker particles shown in (a) as a function of overall shortening (i.e. displacement of the mobile wall). Widening of the shear zone by progressive development of parallel thrusts. Only part of model is shown.

the strong brittle materials quartz sand and corundum (NGab). On the other hand, the use of weak microbeads with a low coefficient of friction (0.41 and 0.40 for fault initiation and fault reactivation, respectively) as part of the graben fill allowed the normal fault closest to the mobile wall to be slightly reactivated (NGwb, NGwm and NGwt). In these

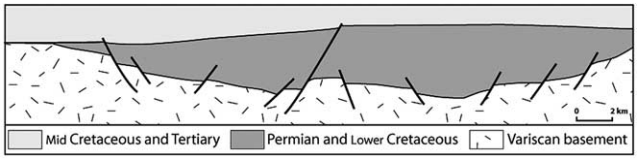

Fig. 11. Part of seismic line SWAT 4, southern Irish Sea, with simplified geological interpretation. Permian, Cretaceous and Tertiary sediments are warped upwards above an earlier faulted extensional basin (modified from Chadwick (1993)).

experiments, reactivation begins in the deeper part of the normal fault and then propagates upward through the post-rift sequence with a shallower dip and/or branches into the footwall.

In their analogue experiments, Huyghe and Mugnier (1992) determine the potential of any part of a fault to be reactivated. Some of their reverse faults use the pre-existing normal fault at depth and then branch off in the shallower part of the model. They show that local weakening along a fault zone decreases the overall faults strength and thus increases the likelihood of its reactivation. Moreover, when located at depth, local weakening localises the formation of a new fault from its upper part. In our models, these weak zones are localised around the graben-bounding faults that bring microbeads and quartz sand/corundum into contact. This strong competence contrast localises shortcuts that develop from the upper part of the microbeads layer. The dip of these shortcut thrusts is lower than that of the reactivated normal fault.

The shallow dip of the continuation of the inverted faults propagating through the previously unfaulted cover has been observed on seismic sections from the southern North Sea (Fig. 12) by Badley et al. (1989) and in sandbox model studies on inversion using a rigid central basement block with dipping basement faults (Koopman et al., 1987).

5.3. Shear zone widening and forced folding

In our models, the lower part of the weak microbeads layers localises the initiation of forward thrusts that propagate along the enveloping surface of the faulted blocks This results in the formation of a forced fold in the weak graben fill with an inverted limb even though overall shortening is not very important.

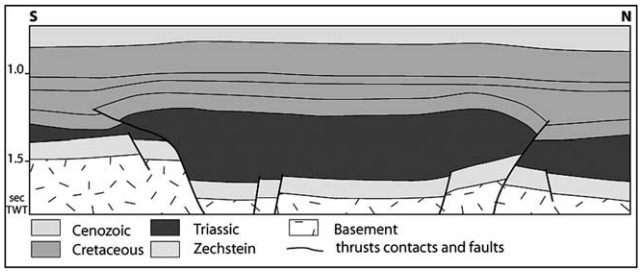

Fig. 12. Line drawing interpretation of a seismic section in the southern North Sea, showing an inverted Triassic basin (modified from Badley et al. (1989)).

The Morcles nappe is a large-scale recumbent fold overlying the Aiguilles Rouges massif in western Switzerland. There is a pronounced thickness change between the Jurassic layers in the core of the Morcles nappe and the underlying thin cover of the Aiguilles Rouges massif (Pfiffner, 1993). This difference in thickness seems to be the result of syn-sedimentary faulting acting during Mesozoic rifting. In accordance with Gillcrist et al. (1987) we interpret the Morcles fold as representing an inverted basin. Another peculiarity is found in its basal thrust, which loses displacement going north and eventually disappears into an anticline–syncline pair in the Tertiary strata as indicated by the geometry of the basal thrust of the Ultra–Helvetic nappes (Fig. 13). This thrust geometry is reminiscent of a fault-propagation fold with a shear zone localised in the strongly deformed lower limb. Without daring to try a direct comparison between the Morcles nappe and our models, we notice the following similarities: both our model structures and the Morcles nappe (1) are linked to the inversion of a basin created during a previous extensional phase, (2) show the development of an inverted limb, and (3) both are the result of the contemporaneous activity of thrusting and folding, a typical feature of a fault-propagation fold.

The formation of a forced fold in the weak graben fill in our experiments is linked to the progressive widening of a shear zone that is composed of several forward thrusts parallel to the enveloping surface of the faulted blocks. Tavarnelli (1997) analysing outcrop-scale structures in a fold-and-thrust belt in the Umbria–Marche Apennines of central Italy interprets the progressive broadening of a thrust-related shear zone during slip as the result of the development of shearing fabrics along the thrust-zone.

5.4. Role of weak zones

In our experiments, shortening is accommodated by structures initiated in zones that deform more easily These

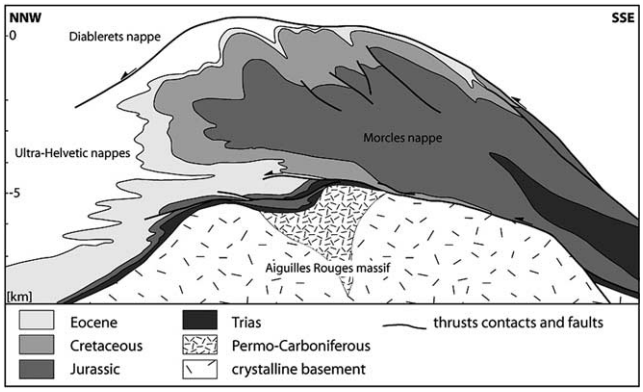

Fig. 13. Cross-section through the Morcles nappe (modified from Pfiffner (1993)).

zones of weakness are localised in the graben fill and are of two types. The first type consists of the weak microbeads that partly fill the graben. During shortening, the graben fill is progressively uplifted and thrust onto the graben-bounding block. This is similar to the northern and central parts of the inverted Broad Fourteens Basin in the southern North Sea (Nalpas et al., 1995; Brun and Nalpas, 1996), where the weak Zechstein salt and its overlying cover are detached from the pre-Permian basement (Fig. 14). In our experiments, the angle between the conjugate forward thrust and backthrust is more or less constant, whereas the location and the dip of the forward thrusts vary as a function of the position of the weak graben fill.

Another zone of weakness is represented by the fault planes. A fault is a narrow dilatant zone along which the sand pack is disturbed: the grains of the granular material are less tightly packed over a width of about 10 times the mean grain size (Panien 2004). The values of friction (Table 1) obtained at the onset of failure (peak strength) and at the moment of fault reactivation (second peak strength) are in agreement with the fact that reactivation of faults occurs at a lower stress value than that required for fault initiation (Krantz, 1991; Lohrmann et al., 2003). In experiment NGab, the competent brittle materials that fill the graben are tightly faulted because of the extension. The forward thrusts that initiate during shortening use this faulted and thus weak zone to propagate. The weak zones created during extension (faults) localise the initiation of new forward- and backthrusts or are partly re-used by newly formed faults. This explains the obliquity of the backthrusts in the case of the oblique graben experiments. Backthrusts are formed progressively, always parallel to the graben axis independent of its orientation with respect to the direction of shortening.

In the case of a partially weak graben fill, the shape of the inverted graben is rather asymmetric, in contrast to the symmetry of the inverted graben with no weak fill (NGab experiment). The graben-fill clearly influences the symmetry of inversion. Bishop and Buchanan (1995), combining fieldwork observations and seismic lines interpretation from the West Coast of South Island (New Zealand), highlight the fact that strong competence contrasts in successive sedimentary units are of importance in controlling the style of basin inversion. For example, thrusts in competent limestones (Oligocene) are decoupled from reverse faults in Precambrian to Palaeocene basement and cover rocks by layers of weak Eocene mudstones, which deform in a quasi-plastic manner. This natural example and our experiments illustrate that the orientation and the position of structural weak zones exert an important control on the nature and style of tectonic reactivation.

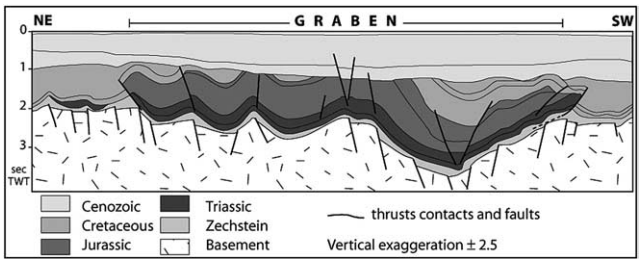

Fig. 14. Line drawing of a seismic section in the Broad Fourteens Basin, North Sea (modified from Nalpas et al. (1995)).

6. Conclusions

Our analogue model experiments simulate the shortening of a graben previously initiated during an extensional phase and progressively filled with brittle materials of different mechanical strengths. The results provide insights into the influence of basin orientation and basin fill on the evolution of structures during inversion. The scaled models contribute to improve our interpretations of inversion-related structures in nature.

The experiments suggest that the presence of weak microbeads inside the graben: (1) enhances reactivation of the major graben-bounding normal fault dipping away from the mobile wall during shortening, (2) localises the development of shortcuts that branch off from this graben-bounding normal fault, (3) determines the location and dip of the main forward thrust that accommodates most of the initial shortening and causes the mechanical extrusion of the graben fill, (4) enhances the overall asymmetry of the inverted graben, and (5) allows the development of a fold in the weak microbeads that evolves by hinge roll and whose formation is linked to the progressive broadening of a shear zone composed of several parallel forward thrusts. In addition, the experiments indicate that the presence of faulted zones inside the graben that were created during extension facilitate the development of forward thrusts during inversion. Thus, both pre-inversion normal faults and microbeads represent weak zones that exert an important control on the location and orientation of structures during inversion. This effect is clearly seen when one considers the effect of the initial orientation of the basin on the resulting structures during inversion. In the case where the long axis of the basin is perpendicular to the shortening direction, the strike of forward- and backthrusts that form during inversion is parallel to the basin. However, when the long axis is oblique to the shortening direction (angle of 60° in the OG experiment), forward- and backthrusts also develop parallel to the basin and thus oblique to the shortening direction.

Acknowledgements

Funding by the Swiss National Science Foundation (project number 2000-067952.02) is gratefully acknowledged. Special thanks to Susanne Buiter for her useful suggestions and comments. A. Liechti and H.P. Bärtschi are thanked for technical assistance, Prof. P. Vock for the use of

the X-ray scanner at the Inselspital in Bern, and C. Seiler and C. Somasundaram for their help in data acquisition. We thank Jo Lohrmann and Christopher Talbot for their constructive reviews.

References

Badley, M.E., Price, J.D., Backshall, L.C., 1989. Inversion, reactivated faults and related structures: seismic examples from the southern North Sea, in: Cooper, M.A., Williams, G.D. (Eds.), Inversion Tectonics Geological Society Special Publication, 44, pp. 201–219.

Barnhoorn, A., Bystricky, M., Burlini, L., Kunze, K., 2004. The role of recrystallisation on the deformation behaviour of calcite rocks: large strain torsion experiments on Carrara marble. Journal of Structural Geology 26, 885–903.

Bishop, D.J., Buchanan, P.G., 1995. Development of structurally inverted basins: a case study from the West Coast, South Island, New Zealand, in: Buchanan, J.G., Buchanan, P.G. (Eds.), Basin Inversion Geological Society Special Publication, 88, pp. 549–585.

Brun, J.P., Nalpas, T., 1996. Graben inversion in nature and experiments. Tectonics 15, 677–687.

Buchanan, P.G., McClay, K.R., 1991. Sandbox experiments of inverted listric and planar fault systems. Tectonophysics 188, 97–115.

Buchanan, P.G., McClay, K.R., 1992. Experiments on basin inversion above reactivated domino faults. Marine and Petroleum Geology 9, 486–500.

Byerlee, J., 1978. Friction of rocks. Pure and Applied Geophysics 116, 615–626.

Chadwick, R.A., 1993. Aspects of basin inversion in southern Britain. Journal of the Geological Society 150, 331–332.

Cloos, E., 1968. Experimental analysis of Gulf Coast fracture patterns. American Association of Petroleum Geologists Bulletin 52 (3), 420–444.

Colletta, B., Letouzey, J., Pinedo, R., Ballard, J.F., Balé, P., 1991. Computerized X-ray tomography analysis of sandbox models: examples of thin-skinned thrust systems. Geology 19, 1063–1067.

Eisenstadt, G., Withjack, M.O., 1995. Estimating inversion: results from clay models, in: Buchanan, J.G.B., Buchanan, P.G. (Eds.), Basin Inversion Geological Society Special Publication, 88, pp. 119–136.

Etheridge, M.A., 1986. On the reactivation of extensional fault systems. Philosophical Transactions of the Royal Society of London, Series A: Mathematical and Physical Sciences 317, 179–194.

Gillcrist, R., Coward, M., Mugnier, J.L., 1987. Structural inversion and its controls: examples from the Alpine foreland and the French Alps. Geodynamica Acta 1, 5–34.

Hubbert, M.K., 1937. Theory of scale models as applied to the study of geologic structures. Bulletin of the Geological Society of America 48, 1459–1520.

Hubbert, M.K., 1951. Mechanical basis for certain familiar geologic structures. Bulletin of the Geological Society of America 62, 355–372.

Huyghe, P., Mugnier, J.L., 1992. Short-cut geometry during structural inversions: competition between faulting and reactivation. Bulletin de la Société géologique, France 163 (6), 691–700.

Keller, J.V.A., McClay, K.R., 1995. 3D sandbox models of positive inversion, in: Buchanan, J.G.B., Buchanan, P.G. (Eds.), Basin Inversion Geological Society Special Publication, 88, pp. 137–146.

Koopman, A., Speksnijder, A., Horsfield, W.T., 1987. Sandbox model studies of inversion tectonics. Tectonophysics 137, 379–388.

Krantz, R.W., 1991. Normal fault geometry and fault reactivation in tectonic inversion experiments, in: Roberts, A.M., Yielding, G., Freeman, B. (Eds.), The Geometry of Normal Faults Geological Society Special Publication 56, 219–229.

Lohrmann, J., Kukowski, N., Adam, J., Oncken, O., 2003. The impact of analogue material properties on the geometry, kinematics and dynamics of convergent sand wedges. Journal of Structural Geology 25, 1691–1711.

Mandl, G., 1988. Mechanics of Tectonic Faulting. Models and Basic Concepts. Elsevier, Amsterdam.

McClay, K.R., 1989. Analogue models of inversion tectonics, in: Cooper, M.A., Williams, G.D. (Eds.), Inversion Tectonics Geological Society Special Publication 44, 41–59.

McClay, K.R., 1995. The geometries and kinematics of inverted fault systems: a review of analogue model studies, in: Buchanan, J.G.B., Buchanan, P.G. (Eds.), Basin Inversion Geological Society Special Publication 88, 97–118

McClay, K.R., Buchanan, P.G., 1992. Thrust faults in inverted extensional basins, in: McClay, K.R. (Ed.), Thrust Tectonics. Chapman and Hall, London, 93–104

McClay, K.R., Ellis, P.G., 1987. Geometries of extensional fault systems developed in model experiments. Geology 15, 341–344.

Mitra, S., 1993. Geometry and kinematic evolution of inversion structures. American Association of Petroleum Geologists Bulletin 77 (7), 1159–1191.

Mitra, S., Islam, Q.T., 1994. Experimental (clay) models of inversion structures. Tectonophysics 230, 211–222.

Nalpas, T., Le Douaran, S., Brun, J.P., Unternehr, P., Richert, J.P., 1995. Inversion of the Broad Fourteens Basin (offshore Netherlands), a small-scale model investigation. Sedimentary Geology 95, 237–250.

Panien, M., 2004. Analogue modeling experiments of basin inversion using well characterised granular materials and comparisons with numerical models. PhD Thesis, University of Berne, Switzerland.

Pfiffner, O.A., 1993. The structure of the Helvetic nappes and its relation to the mechanical stratigraphy. Journal of Structural Geology 15, 511–521.

Ramberg, H., 1981. The role of gravity in orogenic belts, in: McClay, K.R., Price, N.J. (Eds.), Thrust and Nappe Tectonics; International Conference Geological Society of London, Special Publication, 9, pp. 125–140.

Roure, F., Colletta, B., 1996. Cenozoic inversion structures in the foreland of the Pyrenees and Alps, in: Ziegler, P.A.H., Horvath, F. (Eds.), Peri-Tethys Memoir 2: Structure and Prospects of Alpine Basins and Forelands Mémoire du Muséum d'Histoire Naturelle, Paris, 170, pp. 173–209.

Schellart, W.P., 2000. Shear test results for cohesion and friction coefficients for different granular materials: scaling implications for their usage in analogue modelling. Tectonophysics 324, 1–16.

Schreurs, G., Hänni, R., Panien, M., Vock, P., 2003. Analysis of analogue models by helical X-ray computerized tomography, in: Mees, F., Swennen, R., Van Geet, M., Jacobs, P. (Eds.), Applications of X-ray Computed Tomography in the Geosciences Geological Society Special Publication, 215, pp. 213–223.

Schulze, D., 1994. Entwicklung und Anwendung eines neuartigen Ringschergerätes. Aufbereitungs-Technik 35/10, 524–535.

Sibson, R.H., 1985. A note on fault reactivation. Journal of Structural Geology 7 (6), 751–754.

Tavarnelli, E., 1997. Structural evolution of a foreland fold-and-thrust belt. Journal of Structural Geology 19 (3–4), 523–534.

Vially, R., Letouzey, J., Benard, F., Haddadi, N., Desforges, G., Askri, H., Boudjema, A., 1994. Basin inversion along the North African Margin: the Saharan Atlas (Algeria), in: Roure, F. (Ed.), Peri-Tethyan Platforms. Editions Technip, Paris, pp. 79–118.

Weijermars, R., Schmeling, H., 1986. Scaling of Newtonian and non-Newtonian fluid dynamics without inertia for quantitative modelling of rock flow due to gravity (including the concept of rheological similarity). Physics of the Earth and Planetary Interiors 43 (40), 316–330.

Yamada, Y., McClay, K., 2003. Application of geometric models to inverted listric fault systems in sandbox experiments. Paper 1: 2D hanging wall deformation and section restoration. Journal of Structural Geology 25, 1551–1560.